

First Experimental Monitoring of the Three-Dimensional Structure of Toroidal Plasmas Using Multiple Soft X-Ray Imaging Techniques^{*)}

Shinichiro INAGAKI, Akio SANPEI, Takeru INOUE, Natsuki KOJIMA, Ryota TAKAOKA, Takahiro SASAKI and Haruhiko HIMURA

Department of Electronics, Kyoto Institute of Technology, Matsugasaki, Sakyo Ward, Kyoto 606-8585, Japan

(Received 9 January 2023 / Accepted 10 April 2023)

In this study, a previously proposed three-dimensional (3D) tomography method using a multiple-pinhole camera is applied experimentally to detect 3D structures in reversed-field pinch plasmas. The 3D structure of the toroidal plasma was successfully reconstructed and found to be consistent with magnetic field measurements at the plasma's edge. The results also indicate that toroidal mode number estimation may be possible using the images from the multiple-pinhole camera.

© 2023 The Japan Society of Plasma Science and Nuclear Fusion Research

Keywords: imaging measurement, soft x-ray, three-dimensional diagnostics, reversed-field pinch, asymmetric toroidal plasma

DOI: 10.1585/pfr.18.2402046

1. Introduction

Studying the dynamics of self-organized plasmas helps to improve the confinement of high-beta torus plasmas. In reversed-field pinch (RFP) plasmas, the helical equilibrium formed by self-organization can improve confinement [1]. In RFP plasmas, nonlinear interactions between tearing modes produce a stochastic magnetic field that reduces confinement. However, under certain discharge conditions, magnetic energy is concentrated into a single tearing mode. This, in turn, leads to the growth of a magnetic island corresponding to the dominant tearing mode. It also leads to the spontaneous deformation of the magnetic field structure into a helical structure. This phenomenon is referred to as Quasi-Single Helicity (QSH) [2]. In order to better understand QSH and its finer details, a method to accurately monitor the structure of plasma is required.

In our previous studies, RFP plasmas were observed utilizing soft X-ray (SXR) imaging measurements from the tangential direction of the torus [3]. The study implied that both axisymmetric and non-axisymmetric SXR emission profiles existed simultaneously in the torus plasma. Additionally, internal profiles of the magnetic field were measured and showed good agreement with the theoretical helical ohmic equilibrium profiles [4]. However, three-dimensional (3D) structures in the plasma have yet to be directly specified, and a method for estimating 3D structures is still required.

In this study, a 3D tomography method was applied

using a “multiple-pinhole camera,” as described in a feasibility study [5] and preliminary report [6], to detect 3D structures in RFP plasmas. The camera was used to monitor plasma shapes by detecting bremsstrahlung emission in the SXR range, which depends on plasma densities and electron temperatures [7]. For the tomography method, expansion with the Fourier-Bessel (FB) series was utilized. Ridge and Lasso regressions were employed to estimate the coefficients of the FB series. In addition, comparisons between the reconstructed profiles and magnetic field fluctuations measured at the plasma edge are discussed.

2. Experimental Setup

Experiments were conducted in an RFP machine referred to as RELAX [8]. In RELAX, the typical plasma parameters are as follows: toroidal plasma current I_p of 40 - 120 kA with discharge duration of 1.5 - 3.5 ms, line-averaged electron densities n_e of $0.2 - 3 \times 10^{19} \text{ m}^{-3}$, and central electron temperatures T_e of $< 150 \text{ eV}$. Figure 1 is a schematic drawing of the top view of RELAX. RELAX has a torus vacuum chamber with major R and minor a radii that are 508 and 250 mm, respectively. The cross-section of the chamber is circular. The toroidal angles are divided into 16 segments numbered from zero to 15 in intervals of $\pi/8$. There are ports at the top and bottom of RELAX at 14 toroidal locations that are equally spaced except for the zeroth and eighth toroidal angles because two poloidal gaps exist in the chamber. Magnetic probes were installed in all the top (U) and bottom (D) ports except for the 2-D port. The probes measured the time derivative of the magnetic field at the plasma edge in three directions. Averaged toroidal magnetic fields were measured at 16 poloidal

author's e-mail: d3822002@edu.kit.ac.jp

^{*)} This article is based on the presentation at the 31st International Toki Conference on Plasma and Fusion Research (ITC31).

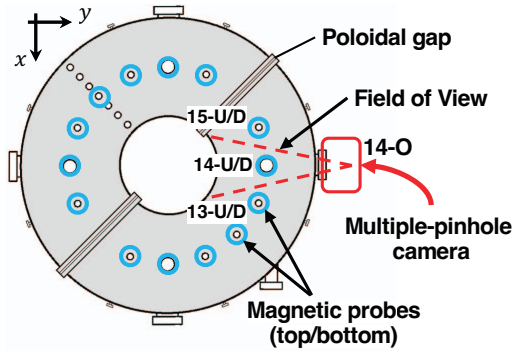


Fig. 1 Schematic top view of RELAX. Blue circles indicate the top and bottom ports where the magnetic probes were inserted. The multiple-pinhole camera is attached to the 14-O port, one of the four ICF152 ports on the equatorial plane of the chamber.

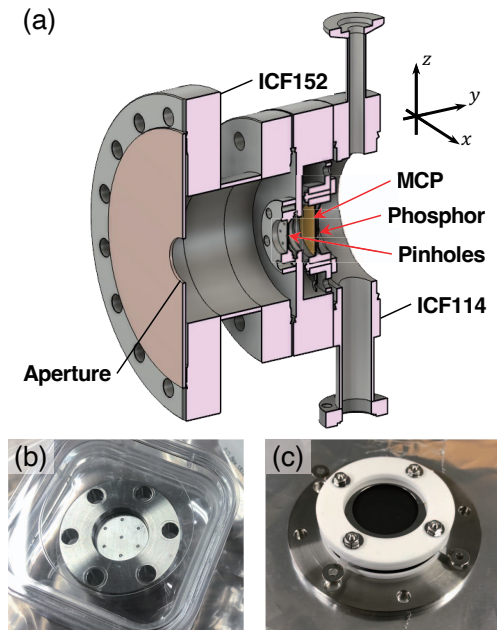


Fig. 2 (a) Cross-sectional view of the multiple-pinhole camera consisting of an aperture, seven pinholes, an MCP, and a phosphor plate. Photographs of the multiple pinholes and the MCP with a phosphor plate are shown in (b) and (c), respectively.

cross-sections via flux loops placed on the outer side of the chamber. The signals from the probes and flux loops were amplified by instrumentation amplifiers and digitized by AD converters. The time evolutions of the magnetic fields were then calculated using numerical integration.

A cross-sectional view of the multiple-pinhole camera is shown in Fig. 2 (a). The multiple-pinhole camera was attached to the 14-O port, represented by a red rectangle in Fig. 1. The port is located on the equatorial plane of RELAX. As a result, the camera's optical axis is along the y -axis. The boundary of the camera's field of view is illustrated by red dashed lines. The multiple-pinhole camera

consists of seven pinholes, an aperture, and a microchannel plate (MCP) with a phosphor plate. As shown in Fig. 2 (b), seven pinholes were drilled into a disk. The disk was located at $y = 945$ mm, 187 mm away from the wall of the chamber. The pinholes were arrayed on the center and circumference of a circle with a radius of 5.3 mm. The hole diameters were 0.5 mm. Since the electron temperature was assumed to be below 150 eV, the camera needed to be sensitive to SXR with low energy, such as wavelengths longer than 10 nm. Therefore, all pinholes were covered with a 1 μm thin aluminum film, allowing the camera to detect SXR appropriately with wavelengths from 20 to 100 nm. Figure 2 (c) shows the MCP and phosphor plate (Hamamatsu Photonics, F2222) assembly. The diameters of the MCP and phosphor plate were 20 and 17 mm, respectively. The distance between the MCP and the disk with the pinholes was 14.3 mm. Regarding the aperture, its diameter was 20 mm, and the distance to the disk with the pinholes was 57.4 mm. Consequently, the distances and diameters of the images produced by the pinholes were approximately 6.6 mm and 5 mm, respectively.

The SXRs emitted from plasmas were converted to visible light by the MCP and phosphor plate. Images appearing on the phosphor plate were recorded with a dynamic range of 12 bits by a high-speed camera (Photron FASTCAM SA-4). The camera captured images at 100 kfps on a 192×128 pixel array. Before analyses, the obtained images were cropped and resized into 32×32 pixels to enlarge the original image in order to decrease the effect of noise via image smoothing. Each pixel in the image was approximately 0.52 mm square. The resulting spatial resolution was 16.5 mm at $y = 508$ mm. The angle of view for a single pinhole and the entire camera was approximately 20 and 30 degrees, respectively.

3. Results

During the experiment, the SXR imaging measurements were taken in an RFP plasma discharge. The plasma current I_p is shown in Fig. 3 (a). Figures 3 (b) and (c) show the time evolutions of the reversed and pinch parameters, F and Θ , defined as:

$$F \equiv \frac{B_t(a)}{\langle B_t \rangle}, \quad \Theta \equiv \frac{B_p(a)}{\langle B_t \rangle}.$$

Where $B_t(a)$ and $B_p(a)$ are the toroidal and poloidal magnetic fields, respectively, as measured by the magnetic probes at the plasma edge, and $\langle B_t \rangle$ is the averaged toroidal magnetic field.

The measurements were taken when the RFPs were in a quasi-steady state with a plasma current of approximately 65 kA. Poloidal magnetic fields were measured at the 13-U/D, 14-U/D, and 15-U/D ports, which were located on the left, center, and right sides of the camera's field of view, respectively. The signals were filtered from 2 to 100 kHz to obtain magnetic field fluctuations \tilde{B} . The $m = 1$ components of \tilde{B} were calculated by subtracting

the bottom values from the top values, where m represents the poloidal mode number. Figures 4 (a), (b), and (c) show \vec{B} and its $m = 1$ component on poloidal cross-sections of

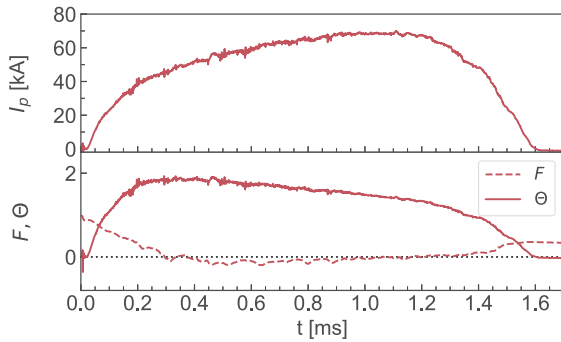


Fig. 3 Time evolutions of I_p (Top), F , and Θ (Bottom). The red solid lines and red dashed lines in the bottom figure indicate F and Θ , respectively. The reconstruction was performed when the I_p was flat-topped, and the plasma was in a quasi-steady state.

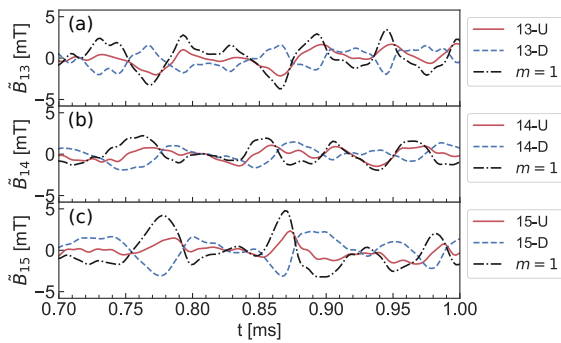


Fig. 4 The magnetic fluctuations measured at (a) $\phi = 13\pi/8$, (b) $14\pi/8$, and (c) $15\pi/8$. For each toroidal angle, the red and blue dashed lines illustrate the values measured at the top (U) and bottom (D), and the black dot-dashed lines show $m = 1$ components obtained by subtracting the top signals from the bottom signals.

$\phi = 13\pi/8$, $14\pi/8$, and $15\pi/8$, respectively. The distinctive peaks of the $m = 1$ component around $t = 0.76$, 0.86 , and 0.97 ms were recognized in all plots. Assuming that the plasma has non-axisymmetric magnetic structures, the cyclic changes in time of the $m = 1$ component of \vec{B} indicate that the plasma rotated in the toroidal direction.

The consecutive images shown in Fig. 5 (a) were captured around $t = 0.85$ ms when the $m = 1$ component at $\phi = 13\pi/8$ had a peak and a direction opposite to that at $\phi = 15\pi/8$. These images contain both axisymmetric and non-axisymmetric components of the SXR emission profiles. Considering the plasma rotates in a toroidal direction, the time-averaged values of luminosities in the images represent the axisymmetric components of the SXR emission profiles in the plasma. In contrast, time-variable values correspond to asymmetric components. Therefore, artificial images shown in Fig. 5 (b) were obtained corresponding to the axisymmetric components in the plasma. The moving average method was employed over the adjacent five images. By subtracting (b) from (a), images that reflect non-axisymmetric structures in the plasma shown in Fig. 5 (c) were obtained.

A 3D reconstruction was performed on the image at $t = 0.86$ ms, highlighted by the red square in Fig. 5. As described in a previous report [6], the FB series' range of modes using the 3D reconstruction was set to $0 \leq m \leq 2$, $-8 \leq n \leq 8$, and $1 \leq k \leq 3$, where the parameters m , n , and k are the poloidal, toroidal, and radial mode numbers, respectively. The coefficients of the FB series were calculated by the Ridge and Lasso regressions, as explained in Ref. [5]. Figure 6 shows the intensities $I_{m,n}$ of the mode spectra estimated by the (a) Ridge and (b) Lasso regressions. For each toroidal and poloidal mode, $I_{m,n}$ is defined as:

$$I_{m,n} = \sqrt{\sum_{k=1}^3 s_{m,n,k}^2},$$

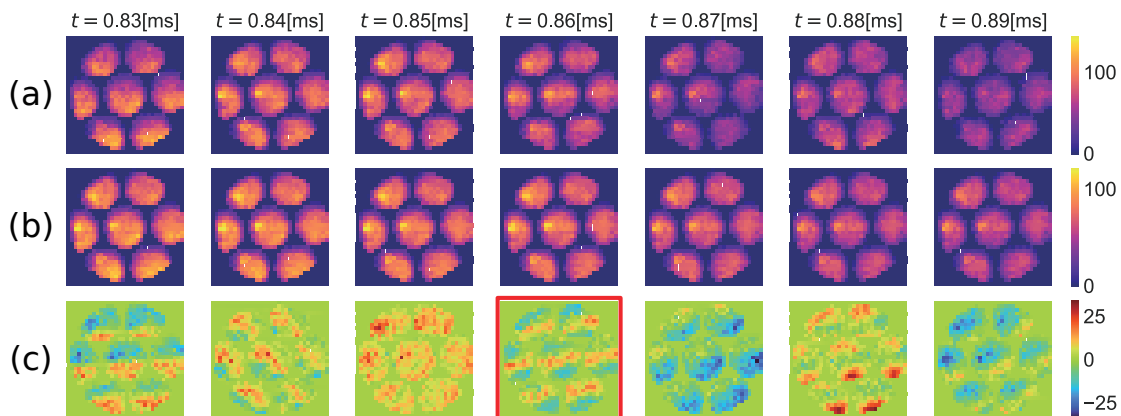


Fig. 5 (a) The time evolution of the images captured by the multiple-pinhole camera, (b) the moving average obtained from the filmed images, and (c) the resultant image calculated by subtracting (b) from (a). The axisymmetric and non-axisymmetric structures of the plasma are reflected in the images shown in (b) and (c), respectively.

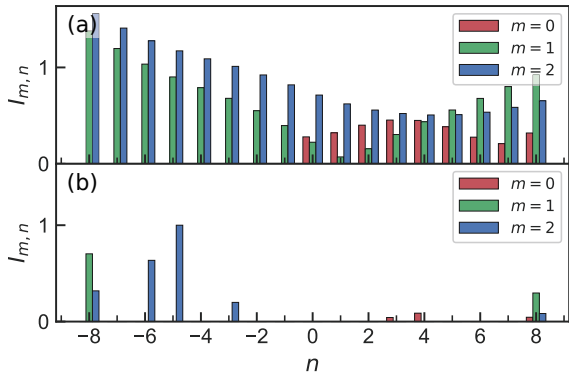


Fig. 6 Dependence of the corresponding $I_{m,n}$ on the poloidal m and toroidal n mode number of the FB series coefficients calculated by (a) Ridge regression and (b) Lasso regression.

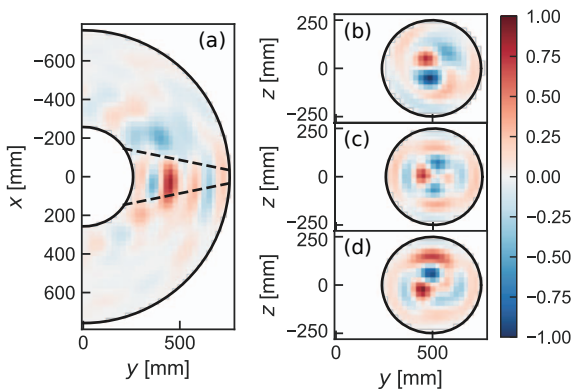


Fig. 7 Reconstructed SXR emission profiles using Ridge regression on (a) the equatorial plane and the yz -planes at (b) $x = -100$ mm, (c) $x = 0$ mm, and (d) $x = 100$ mm.

where $s_{m,n,k}$ is a coefficient corresponding to the FB series with parameters m , n , and k . The values were normalized, with the maximum value of the coefficient being unity. In Fig. 6 (a), the intensity of each mode had a similar order of magnitude, and the higher modes tended to have higher intensities. In contrast, in Fig. 6 (b), narrow spectra were found, and modes with $(m, n) = (1, -8)$, $(2, -5)$, and $(2, -6)$ were dominant.

Figures 7 and 8 show the normalized SXR emission profiles obtained from the coefficients calculated by Ridge and Lasso regressions. The color bar indicates the displacement from the axisymmetric component. For both Fig. 7 and Fig. 8, the profile in (a) the equatorial plane and the profile in the yz -plane at (b) $x = -100$ mm, (c) $x = 0$ mm, and (d) at $x = 100$ mm are shown. Results from both the Ridge and Lasso regressions have a peak around $z = 0$ mm on the yz -plane at $x = 0$ mm. The black dashed lines in (a) illustrate the field of view boundary. There were higher-intensity areas of SXR emission above and below the equatorial plane at $x = -100$ mm and 100 mm, respectively. In (a) of Fig. 7, no periodicity was observed in the toroidal direction. In contrast, the periodicity in the

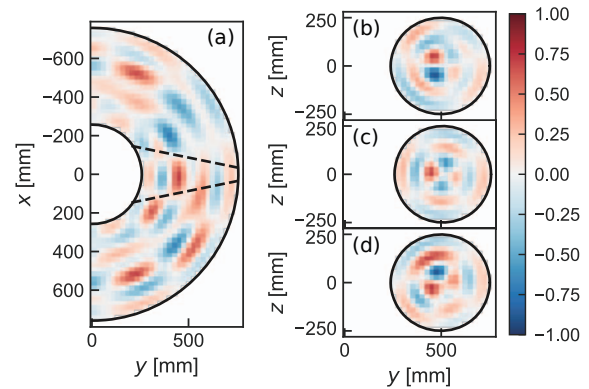


Fig. 8 Reconstructed SXR emission profiles using Lasso regression on (a) the equatorial plane and the yz -planes at (b) $x = -100$ mm, (c) $x = 0$ mm, and (d) $x = 100$ mm.

toroidal direction with $|n| = 5$ or 6 was recognized, in (a) of Fig. 8 because the coefficients estimated by the Lasso regression tend to be sparse, as can also be noted from the spectra in Fig. 6. This feature implies that the toroidal mode numbers can be estimated by Lasso regression. The profiles of the SXR emissions within the field of view were estimated and reproduced in the captured image.

4. Discussion

The reconstructed profiles were compared with the magnetic fluctuations shown in Fig. 4. The $m = 1$ components measured at $\phi = 13\pi/8$ and $15\pi/8$ from $t = 0.85$ to 0.88 ms were positive and negative, respectively. Since the magnetic fluctuations were measured at the top and bottom of a poloidal cross-section, $m = 1$ components of \vec{B} represent vertical shifts of plasma from the equatorial plane, where the upward direction is positive. Therefore, at $\phi = 13\pi/8$ and $15\pi/8$, the plasma was distributed above and below the equatorial plane, respectively. The reconstructed profiles around the field of view were consistent with the edge magnetic field fluctuations. Furthermore, the reconstructed SXR profiles around the field of view were distributed right-handed to the toroidal angle. This direction is consistent with the summation of the toroidal and poloidal magnetic fields produced by the plasma current. These findings suggest that the plasma has non-axisymmetric SXR emission profiles and magnetic structures.

Moreover, the rotation speed of the plasma in the toroidal direction was estimated at approximately 5π rad/ms because peaks existed with a difference of 0.05 ms for $\phi = 13\pi/8$ and $15\pi/8$ at $t = 0.73$ ms and 0.78 ms, respectively. Consequently, the two peaks with a 0.1 ms delay in Fig. 4 (c) were located with an interval of $\pi/2$. The toroidal mode number n may be four. Previous research using nonlinear MHD simulations indicated that the plasma would deform into helical structures with $(m, n) = (1, -4)$ [9], which is consistent with the magnetic

field measurements. While more detailed investigations are required, the obtained profiles show periodicity, which may be correlated to magnetic field fluctuations. However, the dominant modes estimated by Lasso regression were five and six, which is higher than the aforementioned value. The estimated mode numbers tend to be higher than expected, as shown in previous numerical tests in Ref. [5]. The underlying reasons and limitations require further investigation but could be related to the phase of the modes and the wavelength relative to the field of view. Therefore, it is necessary to optimize the size of the aperture and the distances of the pinholes to improve the accuracy of the reconstruction. While the above results indicate that it is possible to estimate the 3D profile of SXR emissions through a single viewing port, improvements may be seen when utilizing a multiple-pinhole camera.

5. Summary

A 3D tomography method was applied using a multiple-pinhole camera to detect 3D structures in RFP plasmas. The 3D structure of the toroidal plasmas was successfully reconstructed and appeared to be consistent with the magnetic fluctuations measured at the plasma's edge. The result from the Lasso regression suggests that it may

be possible to estimate toroidal mode numbers from the images obtained using the multiple-pinhole camera.

Acknowledgments

The authors thank the RELAX team for their helpful discussions and comments. This work was supported by JSPS KAKENHI No. 20KK0063 and No. 21H01056 and by the National Institute for Fusion Science No. NIFS22KIPP016 and No. NIFS20KOAP035, and, in part, by the Joint Usage/Research Program on Zero-Emission Energy Research, Institute of Advanced Energy, Kyoto University ZE2022A-24.

- [1] L. Marrelli *et al.*, Nucl. Fusion **61**, 023001 (2021).
- [2] F. Escande *et al.*, Phys. Rev. Lett. **85**, 3169 (2000).
- [3] T. Onchi *et al.*, Rev. Sci. Instrum. **81**, 073502 (2010).
- [4] K. Oki *et al.*, Plasma Fusion Res. **7**, 1402028 (2012).
- [5] S. Inagaki *et al.*, Nucl. Instrum. Methods Phys. Res. A **1036**, 166857 (2022).
- [6] S. Inagaki *et al.*, Plasma Fusion Res. **18**, 1202010 (2023).
- [7] I.H. Hutchinson, *Principles of Plasma Diagnostics* (Cambridge University Press, 2022).
- [8] S. Masamune *et al.*, J. Phys. Soc. Jpn. **76**, 123501 (2007).
- [9] N. Mizuguchi *et al.*, Plasma Fusion Res. **7**, 2403117 (2012).